Chimeralike states in a minimal network of active camphor ribbons

Jyoti Sharma, Ishant Tiwari, Dibyendu Das, and P. Parmananda
Department of Physics, Indian Institute of Technology - Bombay, Powai, Mumbai, Maharashtra 400076, India

(Received 4 August 2020; accepted 4 January 2021; published 20 January 2021)

A chimeralike state is the spatiotemporal pattern in an ensemble of homogeneous coupled oscillators, described as the emergence of coexisting coherent (synchronized) and incoherent (unsynchronized) groups. We demonstrate the existence of these states in three active camphor ribbons, which are camphor infused rectangular pieces of paper. These pinned ribbons rotate on the surface of the water due to Marangoni effect driven forces generated by the surface tension gradients. The ribbons are coupled via a camphor layer on the surface of the water. In the minimal network of globally coupled camphor ribbons, chimeralike states are characterized by the coexistence of two synchronized and one unsynchronized ribbons. We present a numerical model, simulating the coupling between ribbons as repulsive Yukawa interactions, which was able to reproduce these experimentally observed states.

DOI: 10.1103/PhysRevE.103.012214

I. INTRODUCTION

The study of ensemble dynamics of coupled oscillators has been of wide interest across various disciplines of science. In an ensemble, collective behavior of the oscillators gives rise to fascinating phenomena like pattern formation [1–3], clustering [4,5], amplitude death [6,7], phase flip [8], swarming [9], etc. Besides these, one of the key dynamics is the emergence of synchronization [10], which is the rhythmical behavior of two or more coupled oscillators. Synchronization has been reported in a variety of chemical [5,11,12], physical [13–15], and biological [16,17] systems. In 1975, Kuramoto presented a model for synchronization of phase oscillators [18]. It was then believed that the coupled identical oscillators could either show a synchronized or an unsynchronized state [19].

However, in 2002, Kuramoto and Battogtokh found a remarkable observation for identical phase oscillators [20]. They reported the emergence of coexisting coherent (synchronized) and incoherent (unsynchronized) populations in an ensemble of nonlocally coupled identical oscillators. Although in the past similar coexistence had been reported in some systems [21–24], Abrams and Strogatz were the first to term this coexistence a *chimera* state [25]. Since then, chimera states have been extensively studied both numerically [26–32] and analytically [33,34].

After almost a decade, Tinsley *et al.* observed chimera states in the experiments involving coupled Belousov-Zhabotinsky oscillators [35]. In the same year, Hagerstrom *et al.* found these patterns in coupled map lattices using a liquid crystal spatial light modulator [36]. Recently, chimeras have been experimentally realized in mechanical [37–39], chemical [40], optoelectronic [41], and optical [42] oscillators. Furthermore, some aquatic mammals show chimeralike features related to unihemispheric sleep [43], in which one cerebral hemisphere sleeps while the other is awake. In Ref. [19] a review of the development of chimera states on both experimental and numerical fronts is undertaken.

The numerical investigations of chimera states have been mostly performed on a large ensemble of coupled oscillators. However, for practical purposes, it is crucial to know the minimum number of oscillators that can manifest chimera(like) states. In 2016, Wojewoda *et al.* reported the emergence of a chimera in an experimental setup of three coupled mechanical oscillators [44], where two coherent (synchronized) and one incoherent oscillators coexist. Recently, Awal *et al.* showed numerically a system of only two coupled identical oscillators, which can also support chimera states [45].

To enhance our understanding of the phenomenon in [43], an experimental laboratory setup in the regime of active oscillators is a pertinent problem. Our work is dedicated to one such study. We report the emergence of chimeralike patterns in active rotors. An active rotor is a self-propelled camphor ribbon, which is a rectangular piece of paper with camphor infused in its matrix. The ribbon, when introduced on the surface of the water, exhibits spontaneous motion. This motion is due to the surface tension gradient, caused by the inhomogeneous distribution of the camphor layer around the ribbon [46,47].

In 1860, Tomlinson reported an extensive set of observations involving the motion of camphor on the surface of water [48] while Van der Mensbrugghe, in 1869, explained the mechanism of this motion [46]. For the last three decades, the camphor system has been extensively studied both experimentally and theoretically [49–55]. Camphor is a promising candidate to study the active particles' collective behaviors such as jamming [4] and synchronization [56–59]. Recently, a camphor rotor was realized as a minigenerator of electricity [60].

We have performed experiments on the minimal network of three coupled camphor ribbons. These ribbons were placed on a triangular geometry. The camphor layer around one ribbon interacts with the camphor layer around other ribbons, which leads to the chemical coupling between the ribbons [56,58].

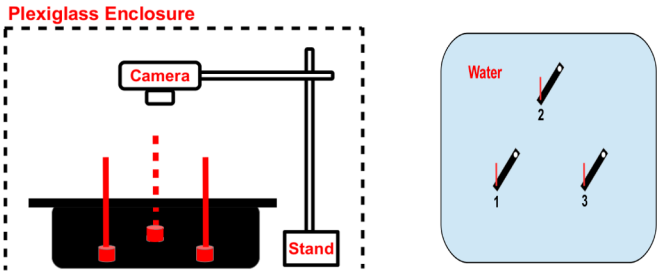

FIG. 1. Sketch of the side view (left) and camera view (right) of the experimental setup for three camphor ribbons placed on the surface of the water in a triangular geometry. The red thin wires represent the needles.

Furthermore, in triangular geometry, each ribbon is uniformly coupled to its nearest neighbors, which results in a global coupling between ribbons.

In the literature, the term "chimera" has been used for both identical [25] and nonidentical [61], nonlocally coupled phase oscillators. Furthermore, in Ref. [40] the terms "chimera" and "chimeralike" have been used for homogeneous and nonhomogeneous globally coupled oscillators, respectively. In real experiments, it is impossible to prepare identical oscillators. Hence, throughout the paper, we use the term "chimeralike" to describe the coexistence of synchronized (coherent) and unsynchronized (incoherent) dynamics of oscillators.

A simulation model of three point particles interacting through a repulsive Yukawa potential [62] is presented. This model was able to reproduce the experimentally observed chimeralike states qualitatively.

This paper is divided into four sections: experiments (Sec. II), the numerical model (Sec. III), discussion (Sec. IV), and conclusions (Sec. V). Furthermore, Sec. II is divided into two subsections that describe the experimental methods and preparation (Sec. II A) and the results (Sec. II B). Similarly, Sec. III is divided into two subsections describing the numerical model (Sec. III A) and the simulation results (Sec. III B).

II. EXPERIMENTS

A. Method and preparation

Figure 1 shows a schematic diagram of the side (left) and camera (right) views of the experimental setup. We performed experiments in a sliced inverted rectangular pyramid shaped glass container. The dimensions of the lower and upper rectangles of the container were 30×20.5 and 34.5×25 cm^2, respectively, while the height was 4.2 cm. This container was placed inside a plexiglass enclosure to prevent air drafts from interfering with the dynamics of the system. The room temperature for all the experiments was set in the range 25.2 °C $\pm$ 0.7 °C. The relative humidity lay between 41% and 46%. A high-speed video camera (GoPro Hero-4, frame rate 120 Hz, 720 p resolution) was installed inside the glass box to record the dynamics of rotators.

For the pivots, we fixed three thin needles (red in Fig. 1), in a regular triangular geometry, on an aluminum sheet which was painted black. Each side of the triangle was equal to 4.2 cm, and the three needles were placed at each of the three vertices. We placed the aluminum sheet fitted with pivots inside the glass container, which was later filled with 1200 mL of water (MilliQ).

Preparation of camphor ribbons. From a clean A4 size paper sheet, three rectangular ribbons with dimensions of 2.0×0.5 cm^2 were cut. The ribbons were kept black in color with a white circular region at one end to aid with the motion tracking of the rotators. A hole was made with a needle at the other end of each paper ribbon. A 3.0 M solution of laboratory grade camphor in ethanol was prepared. One hundred microliters of this solution were poured onto each ribbon. The ribbons were left in the poured solution for 60 s and were then subsequently left to dry in the air for 600 s. Finally, the ribbons were pivoted on the thin needles and were placed on the surface of the water to observe their rotational motion.

The white dots on the ribbons (see the video in the Supplemental Material [63]) were tracked. This tracking and data analysis was performed in a MATLAB interface, using the particle tracking code by Blair and Dufresne [64], which is based on algorithms developed by Crocker and Grier [65]. The positions of the tracked dots are (x_i, y_i), where $i = 1, 2, 3$. For brevity, we will refer to the positions of these white dots as the positions of the ribbons themselves throughout the paper.

B. Results

Three ribbons placed on the triangular geometry can show two main configurations: (1) when all three ribbons are rotating in the same direction and (2) when two of the ribbons are rotating in the same direction and one is rotating in the opposite direction. We denote a pair of corotating (rotating in the same direction) and counterrotating (rotating in the opposite direction) ribbons as $+$ and $-$, respectively. Hence, we label configuration 1 as $+++$ and configuration 2 as $+--$, $-+-$, and $--+$, which are identical configurations except for the different positions of the counterrotating pair [59].

In the smallest network of three ribbons, chimeralike states (CLSs) were observed. The evidence for the emergence of these states is shown in Figs. 2 and 3 for the $+++$ configuration (Video 1 in the SM [63]). The temporal evolution of the x and y positions in Fig. 2 is plotted for 20 s. However, we present the phase plots in Fig. 3 for 100 s. Both temporal evolution [Figs. 2(a) and 2(b)] and the phase plots [Figs. 3(a) and 3(b)] show that the $x(x_1, x_2)$ and $y(y_1, y_2)$ positions of the first and second camphor ribbons are synchronized (refer to Fig. 1 for ribbon number). Phase plots of the $x(x_2, x_3)$ and $y(y_2, y_3)$ positions of the second and third [Figs. 3(c) and 3(d)] camphor ribbons clearly indicate the unsynchronized dynamics between the ribbons. Similarly, Figs. 3(e) and 3(f) show the unsynchronized dynamics of both the $x(x_1, x_3)$ and $y(y_1, y_3)$ positions of the first and third camphor ribbons.

In addition to a CLS, we have observed an unsynchronized state (US), a state where no ribbon pair is synchronized. Typically, a CLS emerged after a US. Moreover, these two states appeared to be robust across different experimental runs. But the time and duration for which a CLS emerges varied across different set of experiments.

Furthermore, both configurations $+++$ and $+--$ ($-+-$, $--+$) were observed. After some initial transient dynamics, the ribbons settle down into one of the two configurations. The initial fluctuations decide the configuration of the

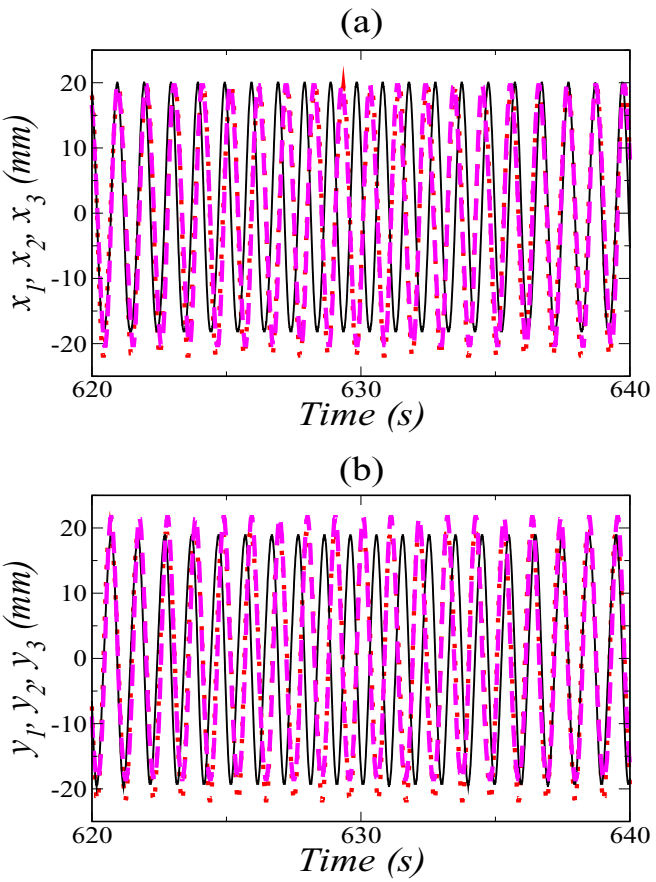

FIG. 2. The temporal evolution of (a) x and (b) y positions of the camphor ribbons for the $+++$ configuration. The red dotted, magenta dashed, and black solid lines correspond to the first, second, and third camphor ribbons, respectively, in both (a) and (b). Ribbon number is mentioned in Fig. 1.

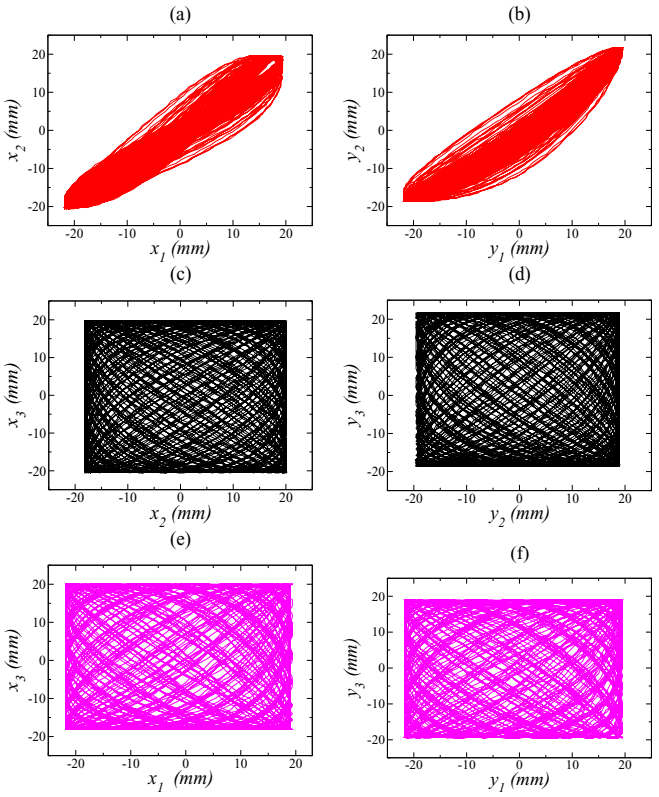

FIG. 3. The phase plots of the x and y positions of the three camphor ribbons for the $+++$ configuration. (a) and (b) The phase plots of the $x(x_1, x_2)$ positions and $y(y_1, y_2)$ positions of the first and second ribbon pairs. (c) and (d) The phase plots of the $x(x_2, x_3)$ positions and $y(y_2, y_3)$ positions of the second and third ribbon pairs. (e) and (f) The phase plots of the $x(x_1, x_3)$ positions and $y(y_1, y_3)$ positions of the first and third ribbon pairs. For ribbon number, see Fig. 1. (x_1, x_2) and (y_1, y_2) are synchronized (coherent), while (x_2, x_3), (y_2, y_3), (x_1, x_3), and (y_1, y_3) are unsychronized (incoherent). This shows the emergence of chimeralike states in the network.

network. But once that choice is made, the ribbons stay in the same configuration for the whole duration of the experiment.

III. SIMULATIONS

A. Model

We consider the camphor ribbons as point particles of unit mass. The point particles are constrained to move along a circle of unit radius. Furthermore, we considered that the center of each circle represents the respective pivot for each ribbon in the experiments.

Three point particles were placed in a triangular geometry with the centers of their respective circles at (0,0), $(\frac{l}{2}, \frac{\sqrt{3}}{2}l)$, and $(l, 0)$ for the first, second, and third point particles. Let (r_i, θ_i) denote the position of the ith $(i = 1, 2, 3)$ particle with respect to the origin (0,0). In the Cartesian coordinate system, the positions of the first, second, and third particles are $(\cos\theta_1, \sin\theta_1)$, $(\cos\theta_2 + \frac{l}{2}, \sin\theta_2 + \frac{\sqrt{3}}{2}l))$, and $(\cos\theta_3 + l, \sin\theta_3)$, respectively.

The point particles interact through a repulsive Yukawa potential. We choose this potential to mimic the experimentally observed repulsive and distance dependent coupling between the ribbons [56]. For a distance $r_{ij}(t)$ between the point particles, the form of the Yukawa potential at any time t is $V(r_{ij}(t)) = \frac{e^{-Kr_{ij}(t)}}{r_{ij}(t)}$, where K is inversely related to the range of the potential. The force due to this potential is $\frac{e^{-Kr_{ij}(t)}}{r_{ij}(t)^2}[1 + Kr_{ij}(t)]$. Furthermore, we assume the radial component of the Yukawa force is balanced by the pivot constraint force. Therefore, only the tangential component of the force acts and determines the dynamics of the particles:

$$F_T(t)_1 = \frac{e^{-kr_{12}(t)}}{r_{12}^3(t)}[1 + kr_{12}(t)]\Big\{\sin[\theta_1(t) - \theta_2(t)] + l\sin\Big[\theta_1(t) - \frac{\pi}{3}\Big]\Big\}$$
$$+ \frac{e^{-kr_{13}}(t)}{r_{13}^3(t)}[1 + kr_{13}(t)]\{\sin[\theta_1(t) - \theta_3(t)] + l\sin\theta_1(t)\}, \quad (1)$$

$$F_T(t)_2 = \frac{e^{-kr_{21}(t)}}{r_{21}^3(t)}[1 + kr_{21}(t)]\Big\{\sin[\theta_2(t) - \theta_1(t)] - l\sin\Big[\theta_2(t) - \frac{\pi}{3}\Big]\Big\}$$
$$+ \frac{e^{-kr_{23}(t)}}{r_{23}^3(t)}[1 + kr_{23}(t)]\Big\{\sin[\theta_2(t) - \theta_3(t)] + l\sin\Big[\theta_2(t) + \frac{\pi}{3}\Big]\Big\}, \quad (2)$$

$$F_T(t)_3 = \frac{e^{-kr_{31}(t)}}{r_{31}^3(t)}[1 + kr_{31}(t)]\{\sin[\theta_3(t) - \theta_1(t)] - l\sin\theta_3(t)\}$$
$$+ \frac{e^{-kr_{32}(t)}}{r_{32}^3(t)}[1 + kr_{23}(t)]\Big\{\sin[\theta_3(t) - \theta_2(t)] - l\sin\Big[\theta_3(t) + \frac{\pi}{3}\Big]\Big\}. \quad (3)$$

The equations governing the dynamics of the ith point particle having natural frequency Ω_i are

$$\dot{\theta}_i(t) = \omega_i(t), \quad i = 1, 2, 3, \quad (4)$$

$$\dot{\omega}_i(t) = F_T(t)_i r_i(t) - C[\omega_i(t) - \Omega_i], \quad i = 1, 2, 3, \quad (5)$$

where the second term in Eq. (5) for $\dot{\omega}_i$ quantifies the tendency of the rotator to go to its autonomous frequency Ω_i if there are no other rotators.

In the experiments, the force experienced by the ribbons does not diverge even at small separations. To incorporate this in the model, we have put a maximum bound $(F_T)_{\max}$ on the magnitude of the total force experienced by each particle [right-hand side of Eq. (5)].

B. Results

We have simulated Eqs. (4) and (5) using the Runga-Kutta fourth-order method with a time step of 10^{-4}. During the simulations, the first 1000 time units were discarded as transients. The system was evolved for the next 1000 time units. The data for these 1000 time units were analyzed, and the corresponding plots for the $+\,+\,+$ configuration are shown in Figs. 4 and 5.

We believe that one can, at best, create quasi-identical ribbons experimentally. Hence, an intrinsic heterogeneity in the ribbons will always be present. To reflect this heterogeneity, in simulations, a slight mismatch in the range [0–0.1], is introduced in the autonomous angular frequencies Ω_i of the point particles. The value of the initial phase θ_i and Ω_i was chosen randomly. The initial value of ω_i was kept equal to its respective autonomous angular frequency Ω_i.

Unlike experiments, here, the initial direction of the rotation of the point particle is not decided randomly. We choose the direction of rotation by setting the sign of Ω_i at the start of the simulations. The configuration $+\,+\,+$ was achieved by keeping the signs of all the Ω_i the same. The other configuration, i.e., $-\,+\,-$ $(+\,-\,-, -\,-\,+)$, can be obtained by reversing the sign of one of the Ω_i.

The value of r_i for $i = 1, 2, 3$ was set to be one unit. The parameters l, K, C, and $(F_T)_{\max}$ were kept constant at 4.0, 1.5, 0.5, and 0.3 units respectively, throughout the simulations.

Figure 4 shows the temporal evolution of the x $[x_i = \cos(\theta_i)]$ and y $[y_i = \sin(\theta_i)]$ positions of all three particles placed in a triangular geometry, while the corresponding phase plots are presented in Fig. 5. Both figures indicate the emergence of CLSs in the simulations where the $x(x_1, x_3)$ and $y(y_1, y_3)$ positions of only the first and third point particles are synchronized. In contrast, the other two pairs remain unsynchronized. Similarly, we have successfully observed the CLS for the other configuration present in this network.

The likelihood of finding a CLS depends upon the initial values of Ω_i [66]. In addition, it was found that regardless of the initial phases, if the autonomous frequencies remained optimally chosen, CLS was observed. Some initial conditions produced only USs. Hence, the point particles performed only either chimeralike or unsynchronized dynamics.

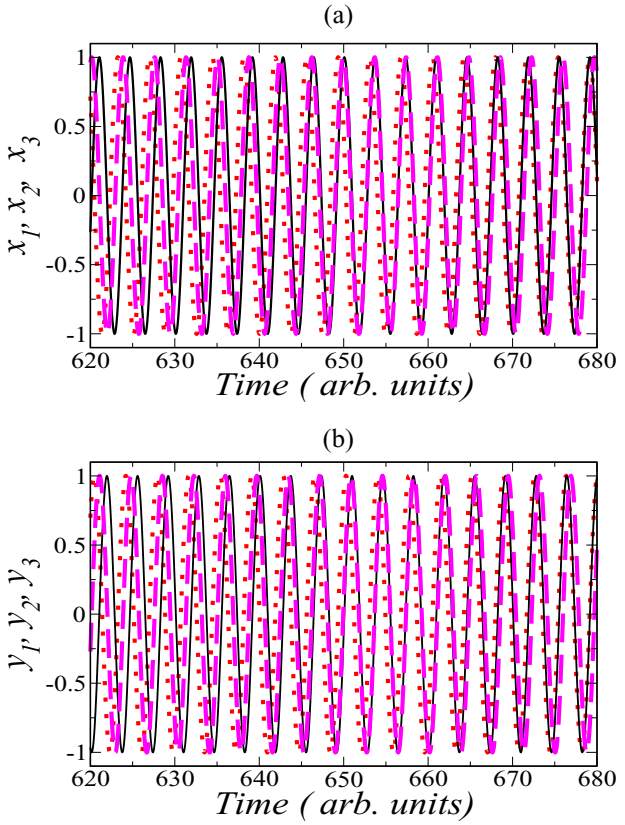

FIG. 4. For the $+\,+\,+$ configuration, the temporal evolution of the (a) $x[x_i = \cos(\theta_i)]$ and (b) $y[y_i = \sin(\theta_i)]$ positions of the point particles placed in a triangular geometry. In both (a) and (b) red dotted, black solid, and magenta dashed lines correspond to the first, second, and third point particles, respectively. Particle number is the same as the ribbon number mentioned in Fig. 1.

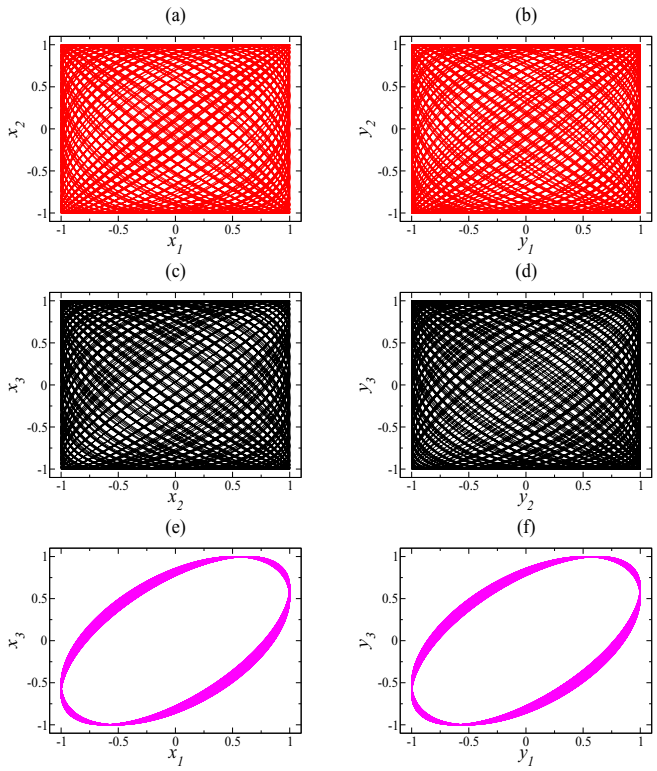

FIG. 5. For the $+\,+\,+$ configuration, the phase plots of the x $[x_i = \cos(\theta_i)]$and y $[y_i = \sin(\theta_i)]$ positions of the three point particles. (a) and (b) The phase plots of the $x(x_1, x_2)$ and $y(y_1, y_2)$ positions of the first and second point particles. (c) and (d) The phase plots of the $x(x_2, x_3)$ and $y(y_2, y_3)$ positions of the second and third point particles. (e) and (f) The phase plots of the $x(x_1, x_3)$ and $y(y_1, y_3)$ positions of the first and third point particle. For particle number, see Fig. 1. (x_1, x_3) and (y_1, y_3) are synchronized (coherent), while (x_2, x_3), (y_2, y_3), (x_1, x_2), and (y_1, y_2) are unsychronized (incoherent).

IV. DISCUSSION

When a camphor infused ribbon touches the water surface, camphor molecules diffuse and form a layer around the ribbon. Any initial inhomogeneity in the distribution of this layer results in a net surface tension gradient around the ribbon and hence rotation of the pinned camphor ribbon. The initial direction of rotation of the ribbon, i.e., clockwise or counterclockwise, is decided randomly. Moreover, once the ribbon starts to rotate in a particular direction, it sustains that direction of rotation, unless perturbed externally. Therefore, the network of three ribbons maintains its initial configuration, i.e., $+\,+\,+$ or $+\,-\,-$ $(-\,+\,-,\ -\,-\,+)$ throughout the experiment.

The camphor layer around one ribbon interacts with the camphor layer around the other two ribbons. This exchange of camphor molecules leads to the chemical coupling between the camphor ribbons. The strength of the coupling is distance dependent [56] and is repulsive.

The chimeralike states in our experiments on globally coupled rotors are different from the relay synchronization states, where two remote and not directly connected (coupled) oscillators are synchronized [67]. Furthermore, it is worth mentioning that the camphor ribbons have a finite life span on the surface of the water. There are two main factors for the slowdown and eventual death of the ribbons. First, as time progresses, the camphor molecules diffused onto the surface of the water from the ribbon cause the fluidic surface to become saturated with camphor. This saturation leads to a decrease in the surface tension gradient and hence a reduced force on the ribbons. Second, ribbons lose their infused camphor due to the finite sublimation rate of camphor at room temperature [47]. This slowdown of ribbons eventually leads to the destabilization of the chimeralike state. Nevertheless, a CLS is relatively stable in comparison to the timescale of the lifetime of the rotational motion. Furthermore, this slowdown of the ribbons is not accounted for in the minimal numerical model involving repulsive Yukawa type interactions. Nonetheless, the simulations reproduced the experimental findings qualitatively.

We believe that our simple experimental setup showing the emergence of chimeralike states in a minimal network of three active oscillators is an interesting contribution to the study of nonlinear aspects of active matter. In the future, one could extend this study in a star network, where the central hub controls the dynamics of the ribbons present at the periphery. To elucidate the phenomenon in [43], where unihemispherical sleep in some mammals was observed, perhaps an experimental setup of two subpopulations of active camphor entities interacting via a fluidic medium could be designed.

V. CONCLUSIONS

We performed experiments on a minimal network of three chemically coupled active oscillators, i.e., camphor ribbons. The camphor ribbons, placed on a triangle, were symmetrically coupled with their nearest neighbors via the camphor layer. In this experimental setup, small chimeralike states emerged, which are characterized by the coexistence of a coherent (synchronized) pair and two incoherent (unsynchronized) pairs of the camphor ribbons. These spatiotemporal patterns are robust across different experiments. We have formulated a point particle model mimicking the coupling between the ribbons as repulsive Yukawa interactions. The numerical simulations qualitatively reproduced the experimentally observed states.

ACKNOWLEDGMENTS

We acknowledge financial support from DST (India; Grant No. EMR/2016/000275). J.S. would like to thank MHRD, India, and IRCC, IITB, India, for financial support. I.T. acknowledges financial support from CSIR, India.

[1] F. G. Kazanci and B. Ermentrout, SIAM J. Appl. Math. **67**, 512 (2007).

[2] P. Parmananda, H. Mahara, T. Amemiya, and T. Yamaguchi, Phys. Rev. Lett. **87**, 238302 (2001).

[3] T. R. Chigwada, P. Parmananda, and K. Showalter, Phys. Rev. Lett. **96**, 244101 (2006).

[4] H. Nishimori, N. J. Suematsu, and S. Nakata, J. Phys. Soc. Jpn. **86**, 101012 (2017).

[5] P. Kumar, D. K. Verma, and P. Parmananda, Phys. Lett. A **381**, 2337 (2017).

[6] R. Phogat, I. Tiwari, P. Kumar, M. Rivera, and P. Parmananda, Eur. Phys. J. B **91**, 111 (2018).

[7] M. Dasgupta, M. Rivera, and P. Parmananda, Chaos **20**, 023126 (2010).

[8] J. M. Cruz, J. Escalona, P. Parmananda, R. Karnatak, A. Prasad, and R. Ramaswamy, Phys. Rev. E **81**, 046213 (2010).

[9] R. van Drongelen, A. Pal, C. P. Goodrich, and T. Idema, Phys. Rev. E **91**, 032706 (2015).

[10] A. Pikovsky, M. Rosenblum, and J. Kurths, *Synchronization: A Universal Concept in Nonlinear Sciences*, Cambridge Nonlinear Sciences Series Vol. 12 (Cambridge University Press, Cambridge, 2003).

[11] J. M. Cruz, M. Rivera, and P. Parmananda, Phys. Rev. E **75**, 035201(R) (2007).

[12] P. Kumar, D. K. Verma, P. Parmananda, and S. Boccaletti, Phys. Rev. E **91**, 062909 (2015).

[13] M. Kapitaniak, K. Czolczynski, P. Perlikowski, A. Stefanski, and T. Kapitaniak, Phys. Rep. **541**, 1 (2014).

[14] A. B. Cawthorne, P. Barbara, S. V. Shitov, C. J. Lobb, K. Wiesenfeld, and A. Zangwill, Phys. Rev. B **60**, 7575 (1999).

[15] Y. Jiang and P. Parmananda, Phys. Rev. E **57**, 4135 (1998).

[16] H. Guo, L. Fauci, M. Shelley, and E. Kanso, J. Fluid Mechanics **836**, 304 (2018).

[17] T. Banerjee and A. Basu, Phys. Rev. E **96**, 022201 (2017).

[18] Y. Kuramoto, in *International Symposium on Mathematical Problems in Theoretical Physics* (Kyoto University, Kyoto/Japan, 1975), pp. 420–422.

[19] M. J. Panaggio and D. M. Abrams, Nonlinearity **28**, R67 (2015).

[20] Y. Kuramoto and D. Battogtokh, Nonlinear Phenom. Complex Systems (Minsk, Belarus) **5**, 380 (2002).

[21] J. P. Crutchfield and K. Kaneko, *Directions in Chaos*, Series on Directions in Condensed Matter Physics Vol. 1 (World Scientific, 1987), pp. 272–353.

[22] P. Parmananda and Y. Jiang, Phys. Lett. A **231**, 159 (1997).

[23] K. Kaneko, Chaos **2**, 279 (1992).

[24] H. Chaté and P. Manneville, Prog. Theor. Phys. **87**, 1 (1992).

[25] D. M. Abrams and S. H. Strogatz, Phys. Rev. Lett. **93**, 174102 (2004).

[26] M. Wolfrum and O. E. Omel'chenko, Phys. Rev. E **84**, 015201(R) (2011).

[27] G. C. Sethia and A. Sen, Phys. Rev. Lett. **112**, 144101 (2014).

[28] S. Sinha, Europhys. Lett. **128**, 40004 (2020).

[29] C. Meena, K. Murali, and S. Sinha, Int. J. Bifurcation Chaos Appl. Sci. Eng. **26**, 1630023 (2016).

[30] B. K. Bera, D. Ghosh, P. Parmananda, G. Osipov, and S. K. Dana, Chaos **27**, 073108 (2017).

[31] F. P. Kemeth, S. W. Haugland, L. Schmidt, I. G. Kevrekidis, and K. Krischer, Chaos **26**, 094815 (2016).

[32] S. Majhi, B. K. Bera, D. Ghosh, and M. Perc, Phys. Life Rev. **28**, 100 (2019).

[33] D. M. Abrams, R. Mirollo, S. H. Strogatz, and D. A. Wiley, Phys. Rev. Lett. **101**, 084103 (2008).

[34] C. R. Laing, Phys. D (Amsterdam, Neth.) **238**, 1569 (2009).

[35] M. R. Tinsley, S. Nkomo, and K. Showalter, Nat. Phys. **8**, 662 (2012).

[36] A. M. Hagerstrom, T. E. Murphy, R. Roy, P. Hövel, I. Omelchenko, and E. Schöll, Nat. Phys. **8**, 658 (2012).

[37] E. A. Martens, S. Thutupalli, A. Fourrière, and O. Hallatschek, Proc. Natl. Acad. Sci. U.S.A. **110**, 10563 (2013).

[38] D. Dudkowski, J. Wojewoda, K. Czołczyński, and T. Kapitaniak, Chaos **30**, 011102 (2020).

[39] P. R. Carvalho and M. A. Savi, Nonlinear Dyn. **102**, 907 (2020).

[40] S. Nkomo, M. R. Tinsley, and K. Showalter, Chaos **26**, 094826 (2016).

[41] L. Larger, B. Penkovsky, and Y. Maistrenko, Phys. Rev. Lett. **111**, 054103 (2013).

[42] J. D. Hart, K. Bansal, T. E. Murphy, and R. Roy, Chaos **26**, 094801 (2016).

[43] N. C. Rattenborg, C. Amlaner, and S. Lima, Neurosci. Biobehav. Rev. **24**, 817 (2000).

[44] J. Wojewoda, K. Czolczynski, Y. Maistrenko, and T. Kapitaniak, Sci. Rep. **6**, 1 (2016).

[45] N. M. Awal, D. Bullara, and I. R. Epstein, Chaos **29**, 013131 (2019).

[46] G. Van der Mensbrugghe, Mém. Couronnés l' Acad. Roy. Sci. Belg. **34**, 1 (1869).

[47] N. J. Suematsu, T. Sasaki, S. Nakata, and H. Kitahata, Langmuir **30**, 8101 (2014).

[48] C. Tomlinson, Proc. R. Soc. London **11**, 575 (1860).

[49] S. Nakata, Y. Iguchi, S. Ose, M. Kuboyama, T. Ishii, and K. Yoshikawa, Langmuir **13**, 4454 (1997).

[50] V. Pimienta and C. Antoine, Curr. Opin. Colloid Interface Sci. **19**, 290 (2014).

[51] S. Nakata, M. Nagayama, H. Kitahata, N. J. Suematsu, and T. Hasegawa, Phys. Chem. Chem. Phys. **17**, 10326 (2015).

[52] M. Nagayama, S. Nakata, Y. Doi, and Y. Hayashima, Phys. D (Amsterdam, Neth.) **194**, 151 (2004).

[53] Y. Koyano, M. Gryciuk, P. Skrobanska, M. Malecki, Y. Sumino, H. Kitahata, and J. Gorecki, Phys. Rev. E **96**, 012609 (2017).

[54] A. Biswas, J. Cruz, P. Parmananda, and D. Das, Soft Matter **16**, 6138 (2020).

[55] M. Frenkel, G. Whyman, E. Shulzinger, A. Starostin, and E. Bormashenko, Appl. Phys. Lett. **110**, 131604 (2017).

[56] J. Sharma, I. Tiwari, D. Das, P. Parmananda, V. S. Akella, and V. Pimienta, Phys. Rev. E **99**, 012204 (2019).

[57] S. Nakata, K. Kayahara, M. Kuze, E. Ginder, M. Nagayama, and H. Nishimori, Soft Matter **14**, 3791 (2018).

[58] M. I. Kohira, Y. Hayashima, M. Nagayama, and S. Nakata, Langmuir **17**, 7124 (2001).

[59] J. Sharma, I. Tiwari, D. Das, P. Parmananda, and V. Pimienta, Phys. Rev. E **101**, 052202 (2020).

[60] M. Frenkel, A. Vilk, I. Legchenkova, S. Shoval, and E. Bormashenko, ACS Omega **12**, 15265 (2019).

[61] E. Montbrió, J. Kurths, and B. Blasius, Phys. Rev. E **70**, 056125 (2004).

[62] J. Rowlinson, Phys. A (Amsterdam, Neth.) **156**, 15 (1989).

[63] See Supplemental Material at http://link.aps.org/supplemental/10.1103/PhysRevE.103.012214 for an experimental video. This video shows the emergence of the chimeralike states in a network of three coupled pinned camphor ribbons. These ribbons

are placed on the surface of the water in a regular triangular geometry.

[64] D. Blair and E. Dufresne, MATLAB particle-tracking code, http://physics.georgetown.edu/matlab.

[65] J. C. Crocker and D. G. Grier, J. Colloid Interface Sci. **179**, 298 (1996).

[66] Refer to the Supplemental Material [65], where we show the effect of the initialization of each rotator's autonomous frequency on the emergence of the CLSs.

[67] I. Leyva, I. Sendiña-Nadal, R. Sevilla-Escoboza, V. Vera-Avila, P. Chholak, and S. Boccaletti, Sci. Rep. **8**, 1 (2018).